A FINITE DIFFERENCE SIMULATION OF THE 2D SCHRODINGER EQUATION WITH ANALYSIS OF A DOUBLE SLIT EXPERIMENT

ROLAND STEVENSON

1. Introduction

$$\boxed{i\hbar\frac{\partial\Psi(x,t)}{\partial t} = -\frac{\hbar^2}{2m}\nabla^2\Psi(x,t) + V(x,t)\Psi}$$

The time dependent Schrodinger equation (TDSE) is the foundation for the modern analysis of linear quantum phenomena. As such, it describes the evolution of a quantum wave function $\Psi(x,t)$, with respect to a potential $V(x,t)$. Uniquely quantum phenomena such as tunnelling and interference are exhibited by wave functions satisfying the Schrodinger equation. It is the goal of this project to illustrate these phenomena in two dimensions through finite difference techniques.

Finite difference approximations allow us to rewrite the TDSE in a discretized form and thus evolve an arbitrary wave function in time. In the case of two dimensions, a method known as Alternating Direction Implicit (ADI) relies on operator splitting to treat each dimension separately, with second order convergence. Both spatial convergence and temporal convergence need to be considered to assure accuracy of the evolution.

After the evolution is shown to converge one can play with wave functions and potentials *ad infinitum*, as the wave function will behave differently for every potential. For example: if the initial wave function is a stationary state of the potential, it will not change it time; if it is an arbitrary superposition of states in a harmonic oscillator potential, it will move periodically across the potential minimum; if it is a planar wave interacting with a double slit, it will create a measurable interference pattern.

The paper will proceed as follows: Section 1 will introduce the TDSE and outline the ADI finite difference methods used to solve the TDSE. Section 2 discusses convergence issues and shows the convergence of the ADI algorithm. Section 3 illustrates wave functions in a few classic potentials (box, free space, harmonic oscillator). Section 4 contains a more rigorous treatment of the double slit potential- a fundamentally two dimensional potential that requires a two dimensional simulation. Section 5 is a conclusion.

2. Time Dependent Schrodinger Equation

2.1. **Deriving a stable approximation to the TDSE.** The time dependent Schrodinger equation is a complex diffusion equation, the solution of which can be approximated with finite difference methods[5]. The TDSE takes the following form:

$$i\frac{\partial \Psi(\mathbf{x},t)}{\partial t} = -\frac{1}{2}\nabla^2\Psi(\mathbf{x},t) + V(\mathbf{x},t)\Psi(\mathbf{x},t) \tag{1}$$

where units are chosen so that $\hbar = 1$ and $m = 1$

Defining the hamiltonian operator

$$\hat{H} = -\frac{1}{2}\nabla^2 + V(x)$$

allows us to write Eq. (1) as

$$i\frac{\partial \Psi(\mathbf{x},t)}{\partial t} = \hat{H}\psi(\mathbf{x},t) \tag{2}$$

Solutions to this equation take the form

$$\Psi(\mathbf{x},t) = e^{-i\hat{H}t}\psi(\mathbf{x},0) \tag{3}$$

This formulation of the solution provides an intuitive paradigm for solving the TDSE: once initial conditions are specified at $t = 0$, the wave function at a time Δt later is computed by calculating $e^{-i\hat{H}\Delta t}\psi(\mathbf{x},0)$. The problem thus reduces to finding an accurate (second order), unitary approximation of $e^{-i\hat{H}\Delta t}$.

Whereas one might be inclined to Taylor expand $e^{-i\hat{H}\Delta t}$ as:

$$e^{-i\hat{H}t} = 1 + i\Delta t\hat{H} + ...$$

it turns out this expansion does not yield unitary (see [5]) evolution. A unitary expansion is found via *Cayley's form*[5]:

$$e^{-i\hat{H}t} = \frac{1 - \frac{1}{2}i\Delta t\hat{H}}{1 + \frac{1}{2}i\Delta t\hat{H}} \tag{4}$$

Finally, using Eq. 4 in Eq. 3, our solution to the TDSE can be written as:

$$(1 + \frac{1}{2}i\Delta t\hat{H})\psi(x, t + \Delta t) = (1 - \frac{1}{2}i\Delta t\hat{H})\psi(x,t) \tag{5}$$

2.2. **Finite Difference Approximation.** Some notation is required to describe the discrete nature of finite difference approximations (FDA). A continuous wave function $\psi(x,y,t)$ can be approximated as evolving values at points on a two dimensional grid. Written in discrete notation, $\psi(x,y,t)$ becomes $\psi^n_{i,j}$, where the i, j indices refer to spatial coordinates and n refers to a temporal one. Using this notation,we can refer to a wave function's value at any point in space and time, including relative locations. For instance, $\psi^n_{i,j+1}$ is ψ's value one grid point away along the positive j-direction.

We are now left to find a FDA of Eq. 5. For all intents and purposes, this amounts to finding a FDA for the Hamiltonian operator, $\hat{H} = -\frac{1}{2}\nabla^2 + V(x)$, which is a composition of the spatial ∇^2 operator and the potential.

The potential operator is easy to approximate, as it is just the value of the potential. If we are evaluating $\psi^n_{i,j}$, then the potential at that point is $V^n_{i,j}$. All of the potentials I consider are time independent, so $V^n_{i,j}$ is just $V_{i,j}$.

$\nabla^2\psi$ can be approximated to second order[1] along one dimension as:

$$\triangle_{xx}\psi_{i,j} \equiv \frac{\partial^2}{\partial x^2}\psi = \frac{\psi_{i+1,j} - 2\psi_{i,j} + \psi_{i-1,j}}{\Delta x^2} \tag{6}$$

Thus in two dimensions,

$$\nabla^2\psi_{i,j} \equiv \triangle_{xx}\psi_{i,j} + \triangle_{yy}\psi_{i,j}$$

and, since

$$\hat{H} = -\frac{1}{2}\nabla^2 + V(x)$$

our FDA of $\hat{H}$ becomes

$$\hat{H}_{i,j} = -\frac{1}{2}(\triangle_{xx} + \triangle_{yy}) + V_{i,j} \tag{7}$$

Therefore, our FDA for 5 is:

$$(1 + \frac{1}{2}i\Delta t\hat{H}_{i,j})\psi^{n+1}_{i,j} = (1 - \frac{1}{2}i\Delta t\hat{H}_{i,j})\psi^n_{i,j} \tag{8}$$

2.3. **ADI Method.** The alternating direction implicit (ADI) method allows us to solve a multidimensional PDE by considering each dimension separately. ADI can only be used when the operators involved in the PDE can be split into differential operators that are independent of each other- (by a method fortuitously labelled operator-splitting!). *Apropos*, our Hamiltonian, Eq. 7, is already manifestly split into three portions: $\triangle_{xx}$, $\triangle_{yy}$, and $V_{i,j}$. Therefore, we split our evolution as:

$$\begin{aligned}
(1 - \frac{1}{4}i\Delta t\triangle_{xx})\psi'^{n+1}_{i,j} &= (1 + \frac{1}{4}i\Delta t\triangle_{xx})\psi^n_{i,j} \\
(1 - \frac{1}{4}i\Delta t\triangle_{yy})\psi''^{n+1}_{i,j} &= (1 + \frac{1}{4}i\Delta t\triangle_{yy})\psi'^n_{i,j} \\
(1 + \frac{1}{2}i\Delta tV_{i,j})\psi'''^{n+1}_{i,j} &= (1 - \frac{1}{2}i\Delta tV_{i,j})\psi''^n_{i,j}
\end{aligned}$$

These equations thus provide a discretized method for evolving a wave function at one time to a new wave function at a time Δt later. Along with a set of Dirichlet boundary conditions, both spatial systems of equations are tridiagonal and can be solved with a complex tridiagonal solver. The final step with respect to the potential is merely linear algebra. These equations and their solver were programmed in Fortran[2] and applied to a variety of interesting initial conditions and potentials. In order for the results of each simulation to be trusted, though, the issues of stability and convergence must be addressed.

[1]For a proof using Maple that this is second order, see Appendix A.

[2]Source located at lnx1.physics.ubc.ca/home/roland/Phys410/project/userfriendly/

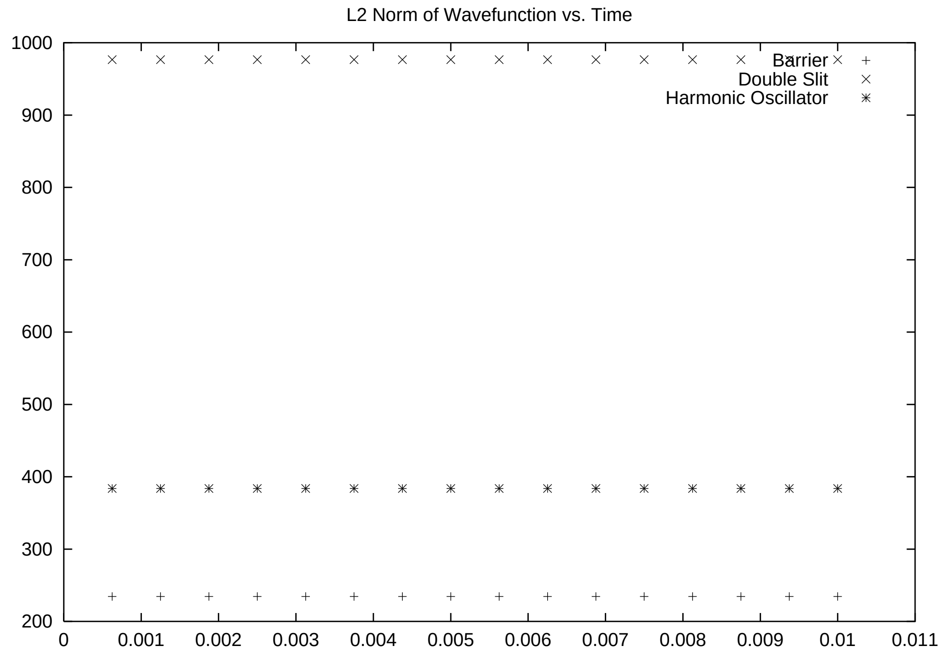

Figure 1

3. Stability and Convergence

3.1. **Stability.** The choice, via Cayley's form (Eq. 4), for the finite difference approximation of $e^{-i\hat{H}t}$ resulted in a claim that the TDSE evolution would be second order and unitary.

We can verify that the evolution is unitary by calculating the L2 norm of the wave function at each point during the evolution, and verifying that it does not change appreciably throughout the simulation.

Fig. 1 illustrates the evolution of the L2 norm for a gaussian pulse in a variety of potentials. Clearly, the L2 norm of the wave function is preserved in a variety of cases[3].

3.2. **Convergence.** If the algorithm is indeed second order, it should converge as such both spatially and temporally. In the former case, we should see that doubling the resolution of our grid results in a four-fold reduction of error in the solution. In the latter case, halving the time-stepping factor should also result in a four-fold reduction of error in the solution. The time-stepping factor, known as the Courant factor, is the ratio

$$\lambda dx = dt$$

The model that was used for spatial and temporal comparison was a gaussian pulse modulated with a plane wave travelling through a zero potential. The solution

[3]The L2-norm has not been normalized to one in each case for illustrative purposes.

was calculated at three different resolutions 40, 80, and 160, which I shall refer to as coarse, medium, and fine, respectively. To be second order convergent the difference between fine and medium should be on the order of one-quarter the difference between medium and coarse.

The results of spatial convergence tests are shown in Appendix C, Figs. 7 and 8 at t=0.005 using a constant Courant factor of 0.001. Fig.7 illustrates the difference between medium and coarse, while 8 illustrates four times the difference between fine and medium. Comparison of the figures illustrates that the differences are of the same form and order, and thus that the algorithm is indeed second order. Similar behavior behavior exists at later times- Figs.9 and 10 illustrate this at t=0.00875.

With respect to temporal convergence, halving the Courant factor (and hence the time-stepping factor), should also result in second order behavior. This behavior is illustrated in Figs.11-14 at times t=0.0025 and t=0.005. In each test, the spatial resolution was held fixed at 320 divisions and the courant factor was reduced by factors of two, yielding solutions at $\lambda = 0.04$(coarse), 0.02(medium), and 0.01(fine). The difference between medium and coarse was on the order of four times the difference between fine and medium in both the t=0.0025 and t=0.005 cases- strongly suggesting second order convergence in time.

One final test is an independent residual test. The test exists in the code I've written, but still has a bug in it. It does not agree with the other convergence tests (L2-norm, spatial, and temporal), which I am inclined to believe. Illustration of and comments on the independent residual test are located in Appendix B.

4. Sample Potentials and Results

4.1. **Particle in an Infinite Square Well.** The simplest potential to look at is the particle in a box. Analytic results state that a particle in an infinite square well potential should have a wave function that is zero at the boundaries and some superposition of eigenfunctions within the domain. For brevity, I skip the derivation and posit that the eigenfunctions are sinusoidal. The state of a particle with an arbitrary superposition of these states would be[2]:

$$\Psi(\mathbf{x},t) = Asin(\frac{n_x\pi}{a}x)sin(\frac{n_y\pi}{a}y) \tag{9}$$

where n_x and n_y correspond to levels of excitation in the x and y directions.

Furthermore, if a wave function is created according to Eq. 9 the L2 norm of the wave function should be constant in time, and we should be able to verify this through our FDA approximation. This can be verified (if one is running DV) by executing the following commands[4]:

- `> setenv DVHOST <yourhost> test`
- `> shro2d 320 20 2 1`
- `> sdftodv *.sdf`

This initializes the $n_x = n_y = 2$ state. Analysis of the **Modpsi** register will show it does not change in time.

[4]These commands should be executed with respect to the executable in lnx1:/home/roland/Phys410/project/userfriendly/

4.2. **Free Space.** Another simple situation to model is that of a gaussian pulse in free space. From Eq. 3, we know that a gaussian should spread out equally in all directions over time, much like a gaussian in the diffusion equation. By running the following commands, we can determine that this is indeed the case.

- `> setenv DVHOST <yourhost> test`
- `> shro2d 320 20 3 1`
- `> sdftodv *.sdf`

Incidentally, if the gaussian were to prefer one direction to another, as was the case at one point during the code's development, it would be a sign that the code was incorrect.

4.3. **Harmonic Oscillator.** One last potential that has been cursorily investigated is the harmonic oscillator which takes the form:

$$V(x,y) = \kappa\, x^2 y^2 \qquad x,y : 0 \leq x \leq 1, 0 \leq y \leq 1$$

where κ is an arbitrary scaling factor. A particle placed in a harmonic oscillator potential will oscillate about the origin with a characteristic frequency that depends on the energy of the particle and κ. If we compute the first spatial moment in each dimension, according to

$$\langle x \rangle = \langle \psi | x | \psi \rangle$$

and

$$\langle y \rangle = \langle \psi | y | \psi \rangle$$

we should see oscillatory motion.

As a test of the simulation with a non-trivial potential, an off-centered gaussian was placed the a harmonic oscillator potential, and $\langle x \rangle$ and $\langle y \rangle$ were computed over time at spatial resolutions of 160, 320, and 640 divisions. The oscillatory motion is exhibited in the Fig. 2 and seems to converge as the number of divisions is doubled.

5. The Double Slit Potential

An interesting application of a two dimensional simulation is the double slit experiment: an electron is fired at a barrier that has two slits in it. It will either reflect off the barrier or pass through one of the two slits. Furthermore, the electron may tunnel through the barrier if the barrier is not infinite.

The double slit potential provides an ideal application for a two dimensional simulation, because the resulting interference pattern cannot be produced in one dimension. Thereby does the development of this ADI code find its vindication.

The test is designed as follows: an 'electron' travelling in the $-\hat{x}$ direction is created by modulating a travelling plane wave with a gaussian envelope. The electron's initial wave function can be described as:

$$\Psi(\mathbf{x}, t) = e^{-\sigma[(x-x_o)^2+(y-y_o)^2]} e^{ikx}$$

The double slit potential is created through a combination of step functions and comprises a barrier at a high potential, with two gaps at zero potential. The gap width and separation[5] can be modified in the source code, but was held constant during the following simulations.

One expects a double slit interference pattern to form as a result of the interaction between the electron and the double slit, and indeed this is the case. However, it

[5]Gap width and separation are input as percentages of the domain width.

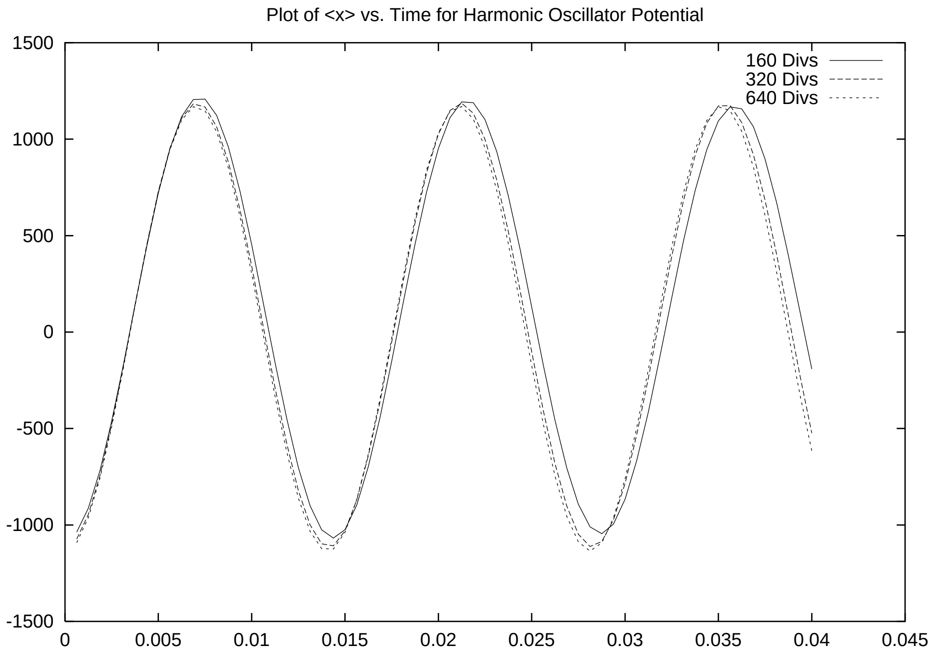

FIGURE 2

is important to note that since we do not have an ideal plane wave, or even a wave equation, the results of an optical double slit do not necessarily hold. We will use this simulation to measure the validity of the optical approximation.

In order to measure the interference pattern the value of the wave function was averaged at the edge of the computational domain (x=0), on the far side of the double slit barrier. The time average of the wave function's L2 norm, $\langle\psi|\psi\rangle$, along the x=0 slice[6] should provide a measure of the resulting intensity as a function of y.

In the limit of geometrical optics, one expects the double slit interference pattern to look like a series of fringes spaced

$$\Delta y = \frac{s\lambda}{a} \tag{10}$$

apart, where s is the distance from the double slit to the measuring plane, and a is the distance between slits. For a good review of this see [7] and [3].

Instead of inputting parameters such as s, a, and λ into Eq. 11 and measuring the fringe separation, Δy, we can look at the dimensionless ratio between the Δy's associated with two wavelengths $\lambda 1$, and $\lambda 2$.

[6]Note that I lied a bit here: Boundary conditions state that at x=0 the wave function must always be zero. So the average was actually taken along a slice near this edge.

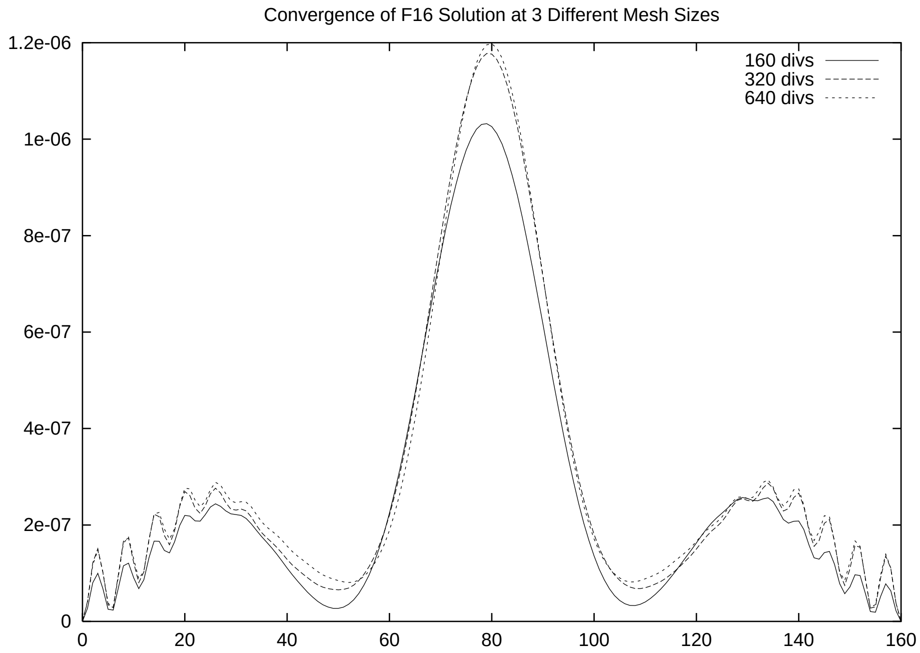

FIGURE 3

Defining $\lambda_2 = \frac{\lambda_1}{2}$, then

$$\frac{\Delta y_1}{\Delta y_2} = 2 \tag{11}$$

and we should be able to confirm this through simulation. It is also noteworthy that if Eq. 11 holds, then the first maximum of λ_2 will occur at the first minimum of λ_1.

The frequency of the plane wave in the code is equal to the wave-number, which is defined as the number of oscillations within the domain; ie. if we choose a frequency of 16, the wave will make 16 full *spatial* oscillations in the domain $0 < x < 1$.

Fig. 3 illustrates the "convergence" of the double-slit interference pattern produced for a wave with a frequency of 16 (F16) at 3 different mesh sizes. Though it does not explicitly show second order convergence, it illustrates that the solution is approaching some limit[7].

The F16 interference pattern shows possible second maxima at x=25 and x=135. One might propose that these second maxima are the result of edge effects, however this is ruled out when one examines higher frequency wave-packets, as follows.

The existence of successive maxima, and the confirmation of Eq. 11 is found when we analyze the interference pattern for multiples of the "fundamental" F16 frequency. The interference pattern is shown in Fig. 4 for F16, F32, and F64.

[7]Note the edge effects produced when the wave packet interacts with the infinite barrier around the domain created by Dirichlet boundary conditions.

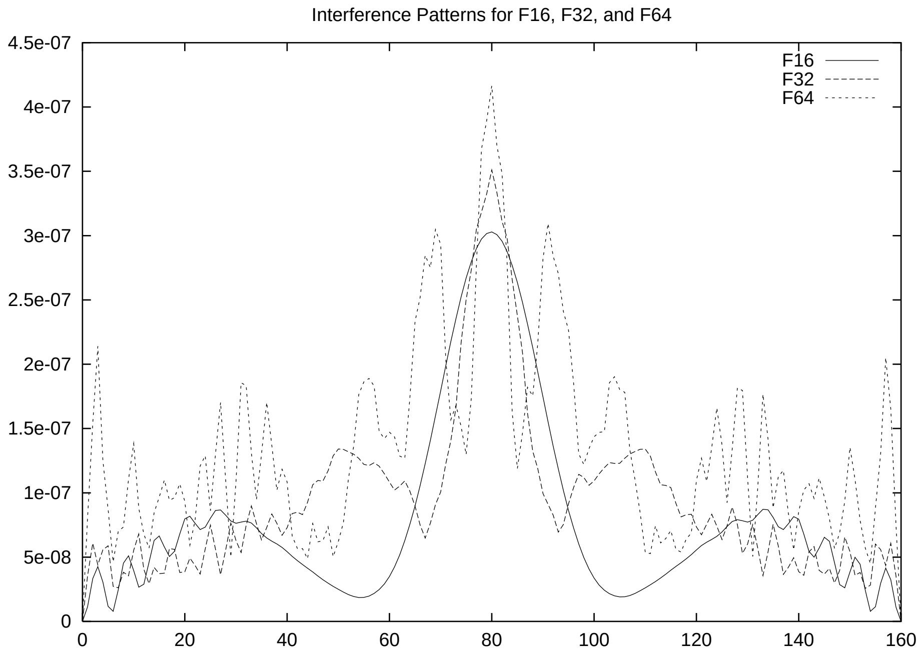

FIGURE 4

As is evident, the ratio of fringe spacing satisfies Eq. 11. We can prove this by measuring the fringe widths for each wave-packet:

$$\Delta_{F16} \approx 45$$
$$\Delta_{F32} \approx 25$$
$$\Delta_{F64} \approx 15$$

and comparing with Eq. 11

$$\frac{\Delta_{F16}}{\Delta_{F32}} \approx \frac{\Delta_{F32}}{\Delta_{F64}} \approx 2$$

We can also note that, as predicted, the first maximum of F32 occurs near the first minimum of F16, and likewise for F64 and F32.

Thus our simulation exhibits behavior consistent with geometrical optics, despite it being derived from a purely quantum mechanical foundation!

6. Conclusion

The purpose of this project was to familiarize myself with the tools and techniques used in the development and analysis of finite difference techniques. The Schrodinger equation provided a background on which to conduct simulations with known solutions.

Implementation of a finite difference code in fortran for the 2D Schrodinger equation yielded some insight into two dimensional methods such as ADI. Though multigrid is the standard, ADI was at least an introduction. Important issues such as stability and convergence were addressed, and the code was shown to be second order both by means of a convergence test and, in the case of a zero potential, an independent residual test.

Finally, the code was tested against known solutions such as the particle in a box, free space, and harmonic oscillator, and then used to simulate a uniquely two dimensional phenomenon- interference patterns from wave packets.

Though all results agreed with expectations, the simulation could still be refined significantly:

- The edge effects evident in interference patterns could be remedied by imposing annihilation boundary conditions.
- The method used to integrate the probability on a slice was not entirely correct. The probability amplitude depended on the grid resolution, and thus required manual normalization to produce Fig. 4
- Finally, the independent residual test exhibited second order convergence with zero potential, but not convincing second order convergence with a non-zero potential such as the harmonic oscillator. This is further explained in Appendix B

Appendix A. Maple Proof of $O(h^2)$ convergence

Verification that the finite difference approximation given in Eq. 6 really does provide $O(h^2)$ approximations of u_{xx}:

- *Taylor expand the function $u(x)$ about x:*

```
> ux := convert(taylor(u(x), h, 8), polynom);
```

$$ux := \mathrm{u}(x)$$

- *Taylor expand it about x+h:*

```
> uxph := convert(taylor(u(x+h),h,8), polynom);
```

$$uxph := \mathrm{u}(x) + \mathrm{D}(u)(x)\,h + \frac{1}{2}\,(\mathrm{D}^{(2)})(u)(x)\,h^2 + \frac{1}{6}\,(\mathrm{D}^{(3)})(u)(x)\,h^3 + \frac{1}{24}\,(\mathrm{D}^{(4)})(u)(x)\,h^4 + \frac{1}{120}\,(\mathrm{D}^{(5)})(u)(x)\,h^5 + \frac{1}{720}\,(\mathrm{D}^{(6)})(u)(x)\,h^6 + \frac{1}{5040}\,(\mathrm{D}^{(7)})(u)(x)\,h^7$$

- *Taylor expand it about x-h:*

```
> uxmh := convert(taylor(u(x-h),h,8), polynom);
```

$$uxmh := \mathrm{u}(x) - \mathrm{D}(u)(x)\,h + \frac{1}{2}\,(\mathrm{D}^{(2)})(u)(x)\,h^2 - \frac{1}{6}\,(\mathrm{D}^{(3)})(u)(x)\,h^3 + \frac{1}{24}\,(\mathrm{D}^{(4)})(u)(x)\,h^4 - \frac{1}{120}\,(\mathrm{D}^{(5)})(u)(x)\,h^5 + \frac{1}{720}\,(\mathrm{D}^{(6)})(u)(x)\,h^6 - \frac{1}{5040}\,(\mathrm{D}^{(7)})(u)(x)\,h^7$$

- *Evaluate the finite difference approximation:*

```
> simplify( (uxph - 2*ux + uxmh)/(h^2) );
```

$$(\mathrm{D}^{(2)})(u)(x) + \frac{1}{12}\,(\mathrm{D}^{(4)})(u)(x)\,h^2 + \frac{1}{360}\,(\mathrm{D}^{(6)})(u)(x)\,h^4$$

- *Clearly, the difference between two solutions will be $O(h^2)$.*

Appendix B. Independent Residual Test

Fig. 5 shows the familiar second order behavior of the simulation for a stationary state of the infinite well potential. With a zero potential inside the box, the independent residual is clearly second order: the independent residual decreases by a factor of four when the mesh spacing is halved.

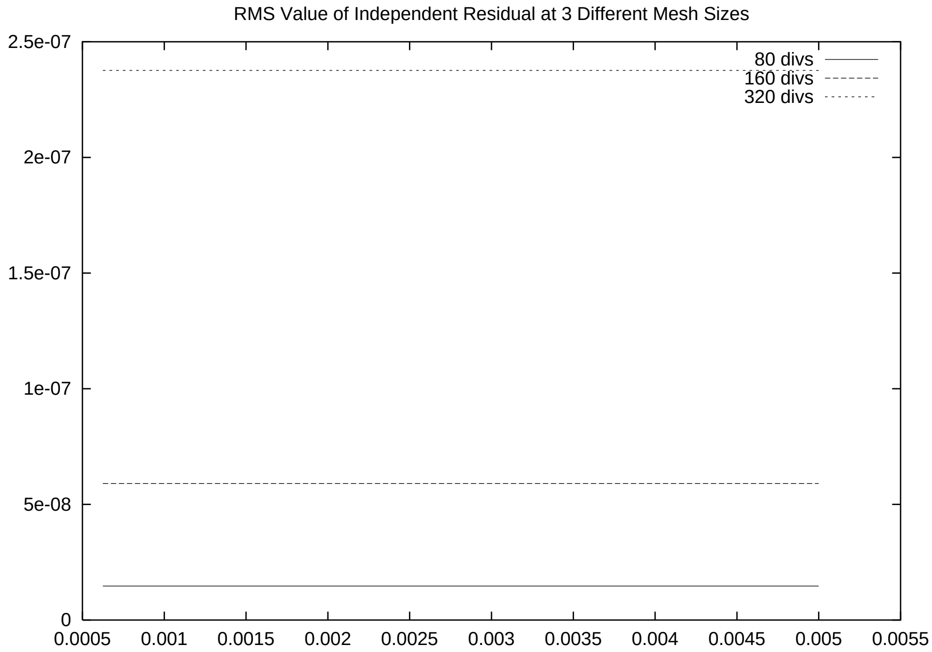

Figure 5

When we switch to a non-zero potential, as in Figure 6, the independent residual behaves differently. The illustrated case is a gaussian in a harmonic oscillator potential. Two important aspects need to be addressed: the independent residual is nowhere near zero, and it behaves somewhere between first and second order. Since this is exhibited only when the potential is non-zero, if the calculation of the independent residual is incorrect, then it is the potential term which is incorrect.

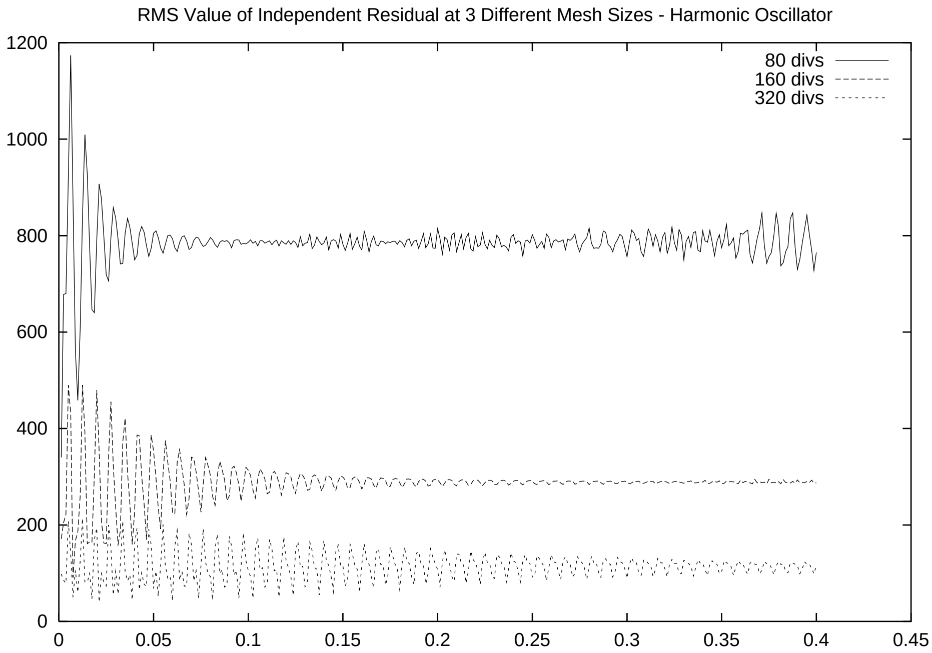

RMS Value of Independent Residual at 3 Different Mesh Sizes - Harmonic Oscillator
80 divs
160 divs
320 divs
1200
1000
800
600
400
200
0
0
0.05
0.1
0.15
0.2
0.25
0.3
0.35
0.4
0.45

FIGURE 6

Appendix C. Convergence Figures

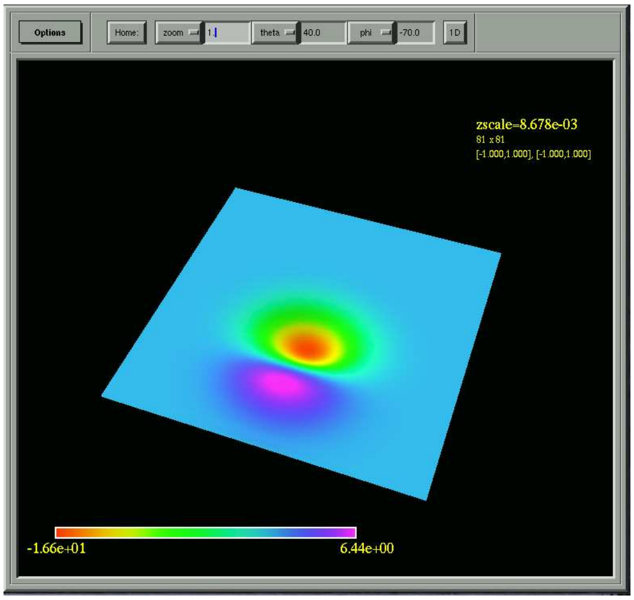

Figure 7. Difference between Coarse and Medium solutions of wave packet travelling over zero potential. t=0.005

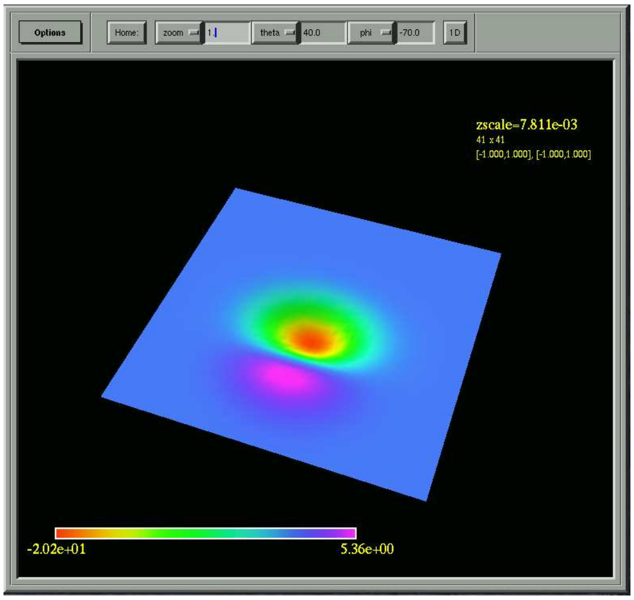

Figure 8. Four times the Difference between Medium and Fine solutions of wave packet travelling over zero potential. t=0.005

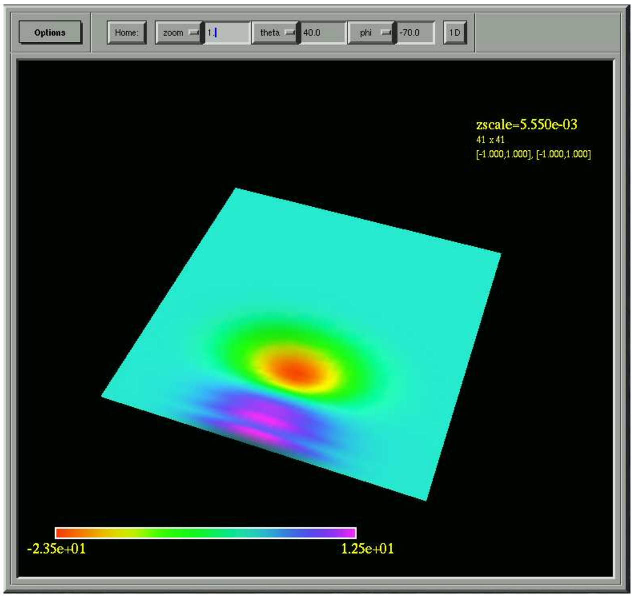

Figure 9. Difference between Coarse and Medium solutions of wave packet travelling over zero potential. t=0.00875

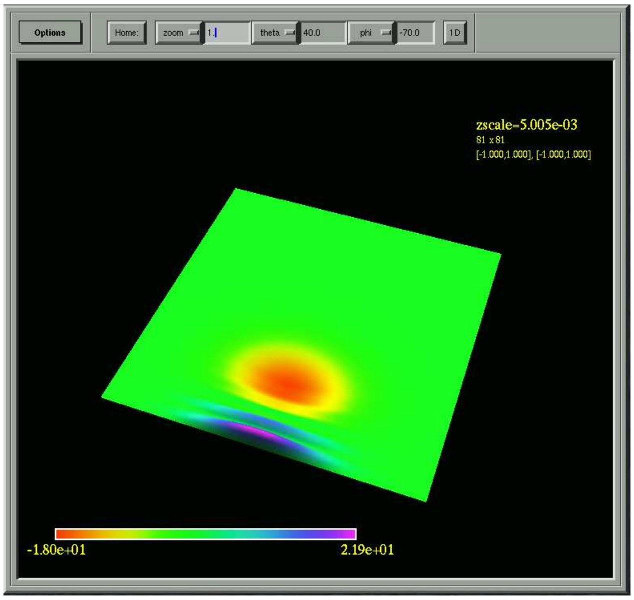

Figure 10. Four times the Difference between Medium and Fine solutions of wave packet travelling over zero potential. t=0.00875

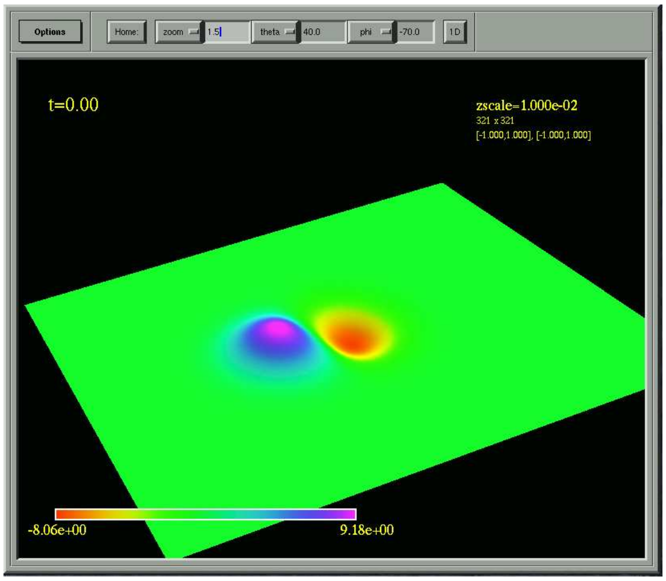

FIGURE 11. Difference between Coarse and Medium solutions of wave packet travelling over zero potential. t=0.0025

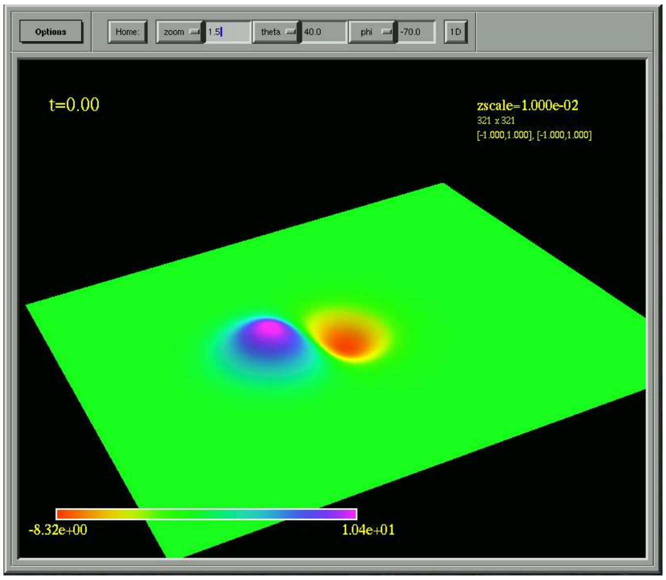

FIGURE 12. Four times the Difference between Medium and Fine solutions of wave packet travelling over zero potential. t=0.0025

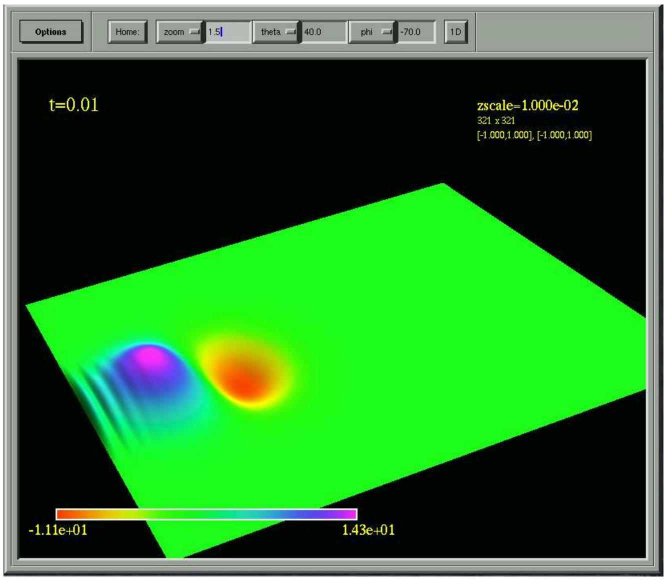

FIGURE 13. Difference between Coarse and Medium solutions of wave packet travelling over zero potential. t=0.005

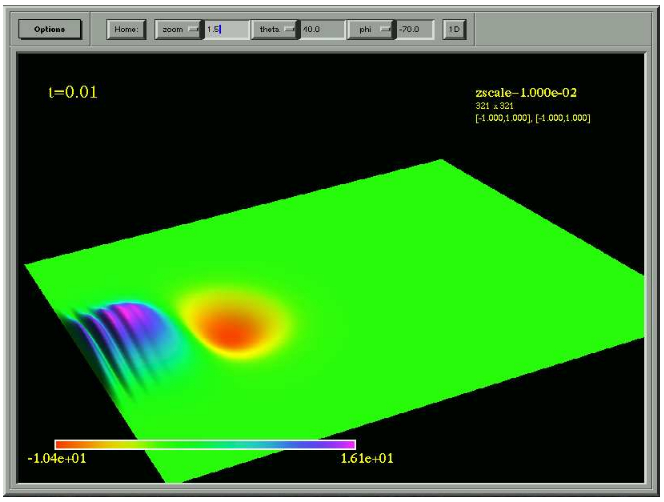

FIGURE 14. Four times the Difference between Medium and Fine solutions of wave packet travelling over zero potential. t=0.005

References

[1] Choi, Dae-Il "Numerical Studies of Nonlinear Schrodinger and Klein-Gordon Systems: Techniques and Applications". University of Texas at Austin, 1998.
[2] Griffiths, David J. "Electromagnetic Fields And Waves," p.26, Prentice Hall, 1995.
[3] Grometstein, A. A. "The Young Experiment (1801)," Ch. 3 in The Roots of Things: Topics in Quantum Mechanics. New York: Kluwer, pp. 65-91, 1999.
[4] Guenther, Reid L. "A Numerical Study of the Time Dependent Schrodinger Equation Coupled with Newtonian Gravity". University of Texas at Austin, 1995.
[5] Press, William H., Flannery, Brian P., Teukolsky, Saul A., Vetterling, William T., "Numerical Recipes in C," p.842, Cambridge University Press., 1986.
[6] Ibid. p.821.
[7] Weisstein, Eric W. "Eric Weisstein's World of Physics" http://scienceworld.wolfram.com/physics/DoubleSlitInterference.html 2003.

E-mail address: `roland@physics.ubc.ca`